WILEY-VCH

DOI: 10.1002/((please add manuscript number))
Article type: Communication

Metal-organic Framework-Activated Carbon Composite Materials for Air Purification

Lauren McHugh, Angela Terracina, Paul Wheatley, Gianpiero Buscarino, Martin Smith and Russell Morris*

L. N. McHugh, Dr. P. S. Wheatley, Prof. R. E. Morris
School of Chemistry, North Haugh, University of St Andrews, St Andrews, KY16 9ST, UK
E-mail: lm83@st-andrews.ac.uk, rem1@st-andrews.ac.uk

A. Terracina, Dr. G. Buscarino
Dipartimento di Fisica e Chimica, Università delgi Studi di Palermo, Palermo, 3690123, Italy

M. W. Smith
CBR Division, Dstl Porton Down, Salisbury, SP4 0JQ, UK

Keywords: porous materials, metal-organic frameworks, activated carbons, gas adsorption, water stability

Metal-organic frameworks (MOFs) are a class of porous materials that show promise in the removal of Toxic Industrial Chemicals (TICs) from contaminated airstreams, though their development for this application has so far been hindered by issues of water stability and the wide availability and low cost of traditionally used activated carbons. Here a series of three MOF-activated carbon composite materials with different MOF to carbon ratios are prepared by growing STAM-17-OEt crystals inside the commercially available BPL activated carbon. The composite materials display excellent water stability and increased uptake of ammonia gas when compared to unimpregnated carbon. Such properties make these composites very promising in the fields of air purification and personal protective equipment.

Metal-organic frameworks (MOFs) are a class of porous, microcrystalline materials that over the last few years have shown potential as adsorbent materials for applications ranging from drug delivery,[1] to gas separation and adsorption.[2] One area where MOFs are of interest is in the removal of toxic industrial chemicals (TICs) such as ammonia and hydrogen sulfide from

airstreams,[3,4] and research is currently underway into the possibility of incorporating MOFs into personal protective equipment, such as respirator canisters.[5]

One of the main issues regarding the potential use of MOFs in personal protective equipment is the hydrolytic stability of the frameworks (due to exposure to the humidity always present in breathable air).[6] Another key problem is the physical form of MOFs in that they typically form fine powders, which a wearer cannot breathe through. This may be addressed by adopting form-altering techniques such as pelletization,[7] though this leads to increased synthetic and engineering costs compared to cheaper, currently used adsorptive materials such as activated carbon. One compromise may be to combine a MOF and activated carbon into a composite material that exhibits positive characteristics from both materials. The growth of MOFs within activated carbons in order to improve the mechanostability of MOFs was reported by Casco,[8] and was further developed by Aurbach to impart electrical conductivity into an otherwise non-conducting MOF.[9] MOFs are chemically good choices for the adsorption of smaller molecules such as ammonia and hydrogen sulfide, due to the strong and selective interactions formed between the framework and the target chemicals. Activated carbons conversely excel in the physisorption of larger molecules such as nerve agents due to their greater porosity and larger pore diameters.[10] By tuning the weight proportion of MOF incorporated into the materials, it is reasonable to suggest that the composites may be tailored to remove specific gases or a broader range of contaminants.

We recently reported the structure of STAM-17-OEt and highlighted its exceptional hydrolytic stability and ability to remove ammonia from both dry and humid airstreams.[11] In this study, we report the synthesis of three novel MOF-carbon composite materials containing STAM-17-OEt and BPL activated carbon. BPL is an unimpregnated coal-based carbon, which is representative of activated carbons that have been used to prepare impregnated carbons such as those often used in respiratory protection.

As shown schematically in **Figure 1**a, the synthesis of MOF-activated carbon composite materials involves two steps: (1) *In situ* synthesis of STAM-17-OEt inside BPL activated carbon particles and (2) Centrifugation and washing of the resulting suspension to afford the STAM-17-OEt@BPL composite materials. This procedure leads to black granular materials that appear to the naked eye similar to unimpregnated carbon samples. Importantly, no 'free' STAM-17-OEt crystals were observed optically, suggesting that the MOF is confined within the carbon. The granular form of the STAM-17-OEt@BPL composites addresses a key issue in the preparation of functional filtration materials, where typically unusable powdered MOF samples have been manufactured into a more useable form by incorporation into a granular activated carbon. Three weight percentages of STAM-17-OEt@BPL are presented here, with 77%, 51% and 39% w/w MOF loading and henceforth named STAM-17-OEt@BPL_1, STAM-17-OEt@BPL_2 and STAM-17-OEt@BPL_3 respectively. The loadings are expressed in weight percentage of MOF, based on an assumed 100% yield of STAM-17-OEt, for example, where 77% loading signifies that each gram of carbon has 0.77 g of MOF added.

Powder X-ray diffraction (Figure 1b) confirms the presence of the parent MOF (STAM-17-OEt) in the composite materials, since some of the crystallinity associated with STAM-17-OEt may be observed along with amorphous character arising from the carbon. The characteristic peaks associated with STAM-17-OEt are present in the composite samples and the relative peak positions are unchanged. MOF may be observed at all three MOF loadings, where the sample containing the highest weight percentage of MOF, i.e. STAM-17-OEt@BPL_1, displays the greatest level of crystallinity. STAM-17@OEt_BPL_3 shows considerably less intensity due to the significantly lower quantity of MOF incorporation.

Powder X-ray diffraction (PXRD) proves the presence of MOF crystals in the composite samples, though it does not indicate whether the MOF is incorporated within the carbon granules or exists separately. Scanning electron microscopy (SEM) images (**Figure 2**a,b)

display the overall morphology of the unimpregnated BPL carbon and STAM-17-OEt respectively. The large voids of ~50 µm in BPL carbon are clearly visible and allow synthesis of smaller MOF crystals within the carbon. STAM-17-OEt crystals have hexagonal morphology and are usually observed as stacked hexagons with typically ~20 µm diameter.[11] SEM images and associated copper elemental mapping images of STAM-17-OEt@BPL_1 (Figure 2c,d), STAM-17-OEt@BPL_2 (Figure 2e,f) and STAM-17-OEt@BPL_3 (Figure 2g,h) verify the fairly even distribution of copper and therefore STAM-17-OEt throughout the carbon. Some areas of more concentrated copper are visible on the surface of the materials, and this is especially true of the samples with higher MOF loading, which suggests that a small amount of STAM-17-OEt has crystallised on the outside of the carbon particles. No discrete MOF particles were observed however, further signifying that STAM-17-OEt is largely confined inside the carbon particles.

In order to investigate the effect of MOF incorporation on carbon porosity, nitrogen BET (Brunauer Emmett-Teller) adsorption measurements were performed. BPL activated carbon has a wide pore size distribution, consisting of both micro and mesopores and has a measured surface area of 1209 m^2/g, which is comparable to the literature value of 1200 m^2/g.[12] STAM-17-OEt, like other MOFs, is a microporous material, though has a surprisingly low surface area of 58 m^2/g.[11] The low porosity in STAM-17-OEt is due to the switchable structure of the material, where upon activation, the pores in STAM-17-OEt become constricted by the change in the coordination environment of the copper paddlewheels. The constriction of the pores consequently impacts the porosity, though the low surface area observed for STAM-17-OEt is not representative of the material's overall gas adsorption capability. A significant drop in the porosity of the carbon upon incorporation of the MOF would provide further evidence that STAM-17-OEt is inside the carbon, due to partial pore-blocking by STAM-17-OEt crystals. The surface areas of the composites do fall in-between

those of the MOF and carbon alone, where the higher the MOF content, the lower the surface area (**Table 1**). The greatest loss of porosity is observed in the highest loading sample: STAM-17-OEt@BPL_1, with a percentage decrease of 90% compared to unimpregnated BPL activated carbon.

SEM and BET analyses both suggest that STAM-17-OEt is largely confined to the pores of BPL activated carbon, but to prove whether the MOF is actually inside the carbon, dynamic vapour sorption studies using either cyclohexane or water vapours were performed. Cyclohexane is known to adsorb on the carbon but not the MOF (due to its relatively small pore size); whilst water vapour adsorbs on both, the resulting isotherms are very different in shape. In either case, pre-activated samples were exposed to increasing levels of relative pressure and the associated uptake was measured at each point. Comparison of the adsorption branches in the water isotherms (**Figure 3**a) shows that BPL, STAM-17-OEt and a physical mixture of the two components equivalent to the highest composite carbon:MOF ratio of 1.00:0.77 weighted average all show a similar mass uptake (ca. 15% w/w) at approximately 55% relative humidity (RH). A lower water uptake of ~12% for STAM-17-OEt@BPL_1 is observed at the same level of RH, suggesting that the MOF is 'inside' the composite and therefore the pores, rather than outside as seen in the physical mixture. The shape of the STAM-17-OEt@BPL_1 isotherm is closer to BPL than STAM-17-OEt, though the total water uptake after exposure to 95% RH is closer to that of STAM-17-OEt, showing that the composites show adsorption characteristics arising from both materials.

Adsorption isotherms of cyclohexane are shown in Figure 3b. This molecule has been used as a model physisorbed chemical which is often used to assess the performance of respirator canisters.[13] It has an atomic radius of ~5.8 Å,[14] and the microporous nature of STAM-17-OEt prevents significant uptake of cyclohexane. The abundance of larger micro- and

mesopores found in BPL activated carbon however, leads to a much greater uptake than in the MOF. The isotherms show that in the composite materials some of the carbon is still accessible to cyclohexane, even at the highest MOF loading in STAM-17-OEt@BPL_1, showing that the transport pores are not simply being 'plugged' with MOF.

Both STAM-17-OEt and BPL activated carbon are stable to moisture and it was anticipated that the MOF-carbon composite materials would maintain this water stability. A water adsorption-desorption cycling experiment was employed to investigate this, where a pre-activated sample was exposed to 90% RH in a series of 8 hour cycles.[15] The maximum water uptake (Figure 3c) remains consistent throughout the cycling experiments, suggesting that the composite is stable even in very harsh conditions. Such hydrolytic stability is undoubtedly imperative in this context due to the moisture always present in breathable air.

In order to investigate the TIC gas adsorption capacity of the materials, micro breakthrough experiments were undertaken, using ammonia as the challenge gas. The resulting micro breakthrough curves (**Figure 4**a) show that BPL carbon alone is fairly ineffective in the removal of ammonia – with an ammonia uptake percentage of 0.43% based on sample weight. STAM-17-OEt performs significantly better, adsorbing 4.33% based on the weight of sample. The highest loading MOF-carbon sample STAM-17-OEt@BPL_1 adsorbs 1.78% based on the weight of sample, which is almost halfway between the values for unimpregnated BPL carbon and STAM-17-OEt. The trend across the series may be observed in Figure 4b, where increasing MOF loading in the composites leads to an overall increase in the uptake of ammonia. Comparison of the ammonia uptakes with the loadings of MOF on the composites suggest that ca. 55-60% of the MOF is available for ammonia removal. This indicates that some of the MOF is either not accessible to the ammonia, or becomes inaccessible as a result of the ongoing reaction between ammonia and MOF.

Activated carbon is known to have low effectiveness in removing smaller molecules such as ammonia from airstreams, as it lacks the strong and selective interactions formed between the metals in MOFs and the gases themselves. STAM-17-OEt forms strong and favourable interactions and this makes it much better for the adsorption of gases such as ammonia. This is in contrast to what was observed in cyclohexane adsorption, where higher MOF loading leads to a decrease in cyclohexane uptake. This relationship leads to the postulation that by controlling the amount of MOF in the pores, we can tailor the performance of the composites accordingly.

Electron paramagnetic resonance (EPR) spectra of activated STAM-17-OEt and the STAM-17-OEt@BPL materials were acquired at T= 77 K and 300 K. The spectra were normalized by all instrumental parameters and the estimated mass of STAM-17-OEt present in each sample (**Figure 5**a,b) and normalized by the amplitude of the main peak (Figure 5c,d). The EPR spectra of activated STAM-17-OEt at 77 K (Figure 5a,c), show signals at 25 mT, 480 mT and 600 mT due to a triplet centre arising from the exchange coupling between the two spins (S=1/2) from Cu^{2+} ions within the paddle-wheel structure. The signal at 330 mT is from Cu^{2+} monomers, which are defects formed during synthesis of the material and the large and unresolved signal observed at 300 K (Figure 5b,d) apply to the triplet centres. The appearance of a single symmetric line for such S=1 centres, instead of the expected multi peak resonance, is due to the exchange interaction between the near magnetic paddle-wheels. The strength of this interaction intensifies upon increasing the temperature as a consequence of the population of the S=1 (triplet) state and it is significant at room temperature. The EPR spectra of STAM-17-OEt@BPL samples are however very different. The peaks corresponding to the triplet centres in STAM-17-OEt are no longer present and only a single resonance at both temperatures with similar features is observed. This narrower resonance, centred at ~340 mT, shows a fine structure comprising a multiplet of four lines, originating from the hyperfine

interaction between the electron spin S =1/2 of the Cu^{2+} ion and its nuclear spin I_{Cu} = 3/2. This multiplet was present also in pristine STAM-17-OEt, but was much less evident.

Significant changes were also observed in the EPR spectra of a similar MOF in another hybrid system, where HKUST-1 was confined within mesostructured silica.[16] The changes in the spectra were attributed to the significantly reduced number of neighbouring paramagnetic centres due to the typically widely spaced pores.

The almost total disappearance of the resonances concerning the triplet centres at 77 K suggests a stronger change in the electronic environment of the paddle-wheels with respect to the cited case and it appears that the signal observed at both 77 and 300 K in the STAM-17-OEt@BPL spectra arise from decoupled copper ions. A similar change in the magnetic properties of MOFs upon incorporation into an activated carbon matrix was observed for HKUST-1.[9] The reasons of this apparent decoupling are still unclear, but it appears to be closely linked to the nature of MOF growth inside a porous carbon matrix.

In conclusion, this manuscript shows the synthesis of MOF-carbon composite materials, where STAM-17-OEt has been incorporated into the commercially available BPL activated carbon at a series of loadings. SEM, water adsorption, cyclohexane uptake and EPR suggest that the MOF is formed within the pores of BPL carbon and water adsorption-desorption cycling highlights the hydrolytic stability of the composites. Microbreakthrough experiments show that the MOF-carbon composite materials increase the quantities of ammonia removed from contaminated airstreams compared with the carbon, and cyclohexane uptake shows that the composites can adsorb significantly more cyclohexane than the MOF alone. The granular form of the STAM-17-OEt@BPL composites also overcomes a major hurdle in the engineering of materials used in personal protective equipment, whereby a powdered MOF has been manufactured into a form that can potentially be used inside a filter. These findings suggest that MOF-carbon composites are exciting materials for use in air purification and by

altering the loading of MOF within the composites, the materials may be tailored to remove a broader range of contaminants than the individual components alone.

Experimental Section

Synthesis of STAM-17-OEt@BPL composites: The BPL activated carbon used in this research was supplied by Chemviron Carbon Ltd. STAM-17-OEt@BPL_1 is prepared by suspending BPL activated carbon (244 mg, 20.32 mmol) and 5-ethoxy isophthalic acid (125 mg, 0.60 mmol) in distilled water (10 mL), before stirring at 45 °C for 2 hours. Copper acetate monohydrate (119 mg, 0.60 mmol) is added and stirring is continued at 45 °C for a further 2 hours. The temperature is increased to 95 °C and the mixture is stirred for a further 3 days. The suspension is centrifuged at 6000 rpm for 10 minutes, and the solid is washed with distilled water (15 mL). The centrifuging and washing cycle is repeated a further 3 times, before drying the solid in air. STAM-17-OEt@BPL_2 and STAM-17-OEt@BPL_3 are synthesised using the same procedure and quantity of BPL carbon, and appropriate quantities of STAM-17-OEt precursors: 5-ethoxy isophthalic acid (83 mg and 68 mg respectively) and 1 equivalent of copper acetate monohydrate (79 mg and 65 mg respectively), resulting in composites with 51% and 39% STAM-17-OEt by weight.

Powder X-ray diffraction (PXRD): Diffraction patterns are collected using a PANalytical Empyrean with Cu X-ray tube and primary beam monochromator (CuKα1). Measurements are performed at 298 K and samples do not require activation prior to recording.

Scanning electron microscopy (SEM): SEM images are recorded using a Jeol JSM 5600 SEM.

Surface area determination: Nitrogen BET analysis is performed on STAM-17-OEt samples at 77 K on a Micromeritics ASAP 2020 Surface Area and Porosity Analyzer and the BET

surface areas are calculated using the Rouquerol method. 120 mg samples are activated at 423 K overnight prior to measurement.

Water and cyclohexane adsorption experiments: Water and cyclohexane adsorption are both measured using a Dynamic Vapour Sorption (DVS Advantage Surface Measurement Systems Ltd) apparatus. A sample of material (typically ~20 mg) is placed in a stainless-steel pan and heated to 423 K for 3 hours in dry air to remove residual moisture. For isotherm measurement, the relative pressure within the instrument is gradually increased to in a series of steps to 95%, and the mass of the sample is monitored throughout. The temperature remains constant at 298 K. Humidity cycling experiments are also completed in a DVS system by changing the relative humidity from 0 to 90% every 8 h. The temperature is held constant at 298 K and the mass of the sample is monitored. The duration of the experiment is 120 h (eight full cycles).

Ammonia micro-breakthrough: Ammonia micro-breakthrough testing is performed using a micro-breakthrough apparatus. The set-up allows the testing of porous materials against known concentrations of challenge gases. Samples of ~20 mg are placed on a metal frit inside a sample chamber and ammonia gas at a concentration of 450 ppm is passed through the sample at a flow rate of 55 mL min^{-1}. The effluent concentration is monitored using a photoionization detector (Phocheck Tiger). All experiments are performed at 298 K.

Electron Paramagnetic Resonance (EPR): EPR measurements are performed using a Bruker EMX micro spectrometer, working at a frequency of approximately 9.5 GHz (X-band), with a magnetic-field modulation frequency set at 100 kHz. The spectra are acquired by inserting the EPR glass tube containing the sample inside a Dewar flask. For measurements conducted at 77 K, the Dewar flask was filled with liquid nitrogen.

Supporting Information

Supporting Information is available from the Wiley Online Library or from the author.

Acknowledgements
L.N.M and R.E.M wish to acknowledge the financial support from the EPRSC industrial CASE award (grant EP/N50936X/1). A.T and G.B would like to thank the financial support from the Fondo per il finanziamento delle attività base di ricerca (grant PJ-RIC-FFABR_2017).

Received: ((will be filled in by the editorial staff))
Revised: ((will be filled in by the editorial staff))
Published online: ((will be filled in by the editorial staff))

References

[1] a) A. C. McKinlay, R. E. Morris, P. Horcajada, G. Férey, R. Gref, P. Couvreuer, C. Serre, *Angew. Chem. Int. Ed.* **2010**, *49*, 6260; b) I. A. Lázaro, R. S. Forgan, *Coord. Chem. Rev.* **2018**, *380*, 230

[2] a) R-B. Lin, S. Xiang, H. Xing, W. Zhou, B. Chen, *Coord. Chem. Rev*, **2019**, *378*, 87; b) K. Sumida, D. L. Rogow, J. A. Mason, T. M. McDonald, E. D. Bloch, Z. R. Herm, T-H. Bae, J. R. Long, *Chem. Rev.* **2012**, *112*, 724.

[3] a) G. W. Peterson, G. W. Wagner, A. Balboa, J. Mahle, T. Sewell, C. J. Karwacki, *J. Phys. Chem. C.* **2009**, *113*, 13906; b) E. Barea, C. Montoro, J. A. R. Navarro, *Chem. Soc. Rev*, **2014**, *43*, 5149.

[4] a) L. Hamon, C. Serre, T. Devic, T. Loiseau, F. Millange, G. Férey, G. De Weireld, *J. Am. Chem. Soc.*, **2009**, *131*, 8775; b) J. Antonio Zárate, E. Sánchez-González, T. Jurado-Vázquez, A. Gutiérrez-Alejandre, E. González-Zamora, I. Castillo, G. Maurin, I. A. Ibarra, *Chem. Comm.* **2019**, *55*, 3049.

[5] M. Jacoby, *Chem. Eng. News.* **2014**, *92*, 34-38.

[6] a) N C. Burtch, H. Jasuja, K. S. Walton, *Chem. Rev.*, **2014**, *114*, 10575; b) M. Todaro, G. Buscarino, L. Sciortino, A. Alessi, F. Messina, M. Taddei, M. Ranocchiari, M. Cannas, F. M. Gelardi, *J. Phys. Chem. C.*, **2016**, *120*, 12879.

[7] S. Hindocha, S. Poulston, *Faraday Discuss.*, **2017**, *201*, 113.

[8] M. E. Casco, J. Fernández-Catalá, M. Martínez-Escandell, F. Rodríguez-Reinoso, E. V. Ramos-Fernández, J. Silvestre-Albero, *Chem. Comm.*, **2015**, *51*, 14191.

[9] O. Fleker, A. Borenstein, R. Lavi, L. Benisvy, S. Ruthstein, D. Aurbach, *Langmuir,* **2016**, *32*, 4935.

[10] a) R. Osovsky, D. Kaplan, I. Nir, H. Rotter, S. Elisha, I. Columbus, *Environ. Sci. Technol.* **2014**, *48*, 10912; b) D. Kaplan, L. Shmueli, I. Nir, D. Waysbort, I. Columbus, *Clean*, **2007**, *35*, 172.

[11] L. N. McHugh, M. J. McPherson, L. J. McCormick, S. A. Morris, P. S. Wheatley, S. J. Teat, D. McKay, D. M. Dawson, C. E. F. Sansome, S. E. Ashbrook, C. A. Stone, M. W. Smith, R. E. Morris, *Nat. Chem.*, **2018**, *10*, 1096.

[12] B. P. Russell, M. D. Levan, *Carbon*, **1994**, *32*, 845.

[13] CEN European Normalization Committee, European Norm EN 14387, Respiratory Protective device - gas filters and combined filters - Requirements, testing, marking (BSI British standards, London 2004).

[14] F. D. Magalhães, R. L. Laurence, W. C. Conner, *J. Phys. Chem. B.*, **1998**, *102*, 2317.

[15] J. R. Álvarez, E. Sánchez-González, E. Pérez, E. Schneider-Revueltas, A. Martinez, A. Tejeda-Cruz, A. Islas-Jácome, E. González-Zamora, I. A. Ibarra*, Dalton Trans*, **2017**, *46*, 9192.

[16] M. Mazaj, T. Čendak, G. Buscarino, M. Todaro, N. Zabukovec Logar, *J. Mat. Chem. A.*, **2017**, *5*, 22305

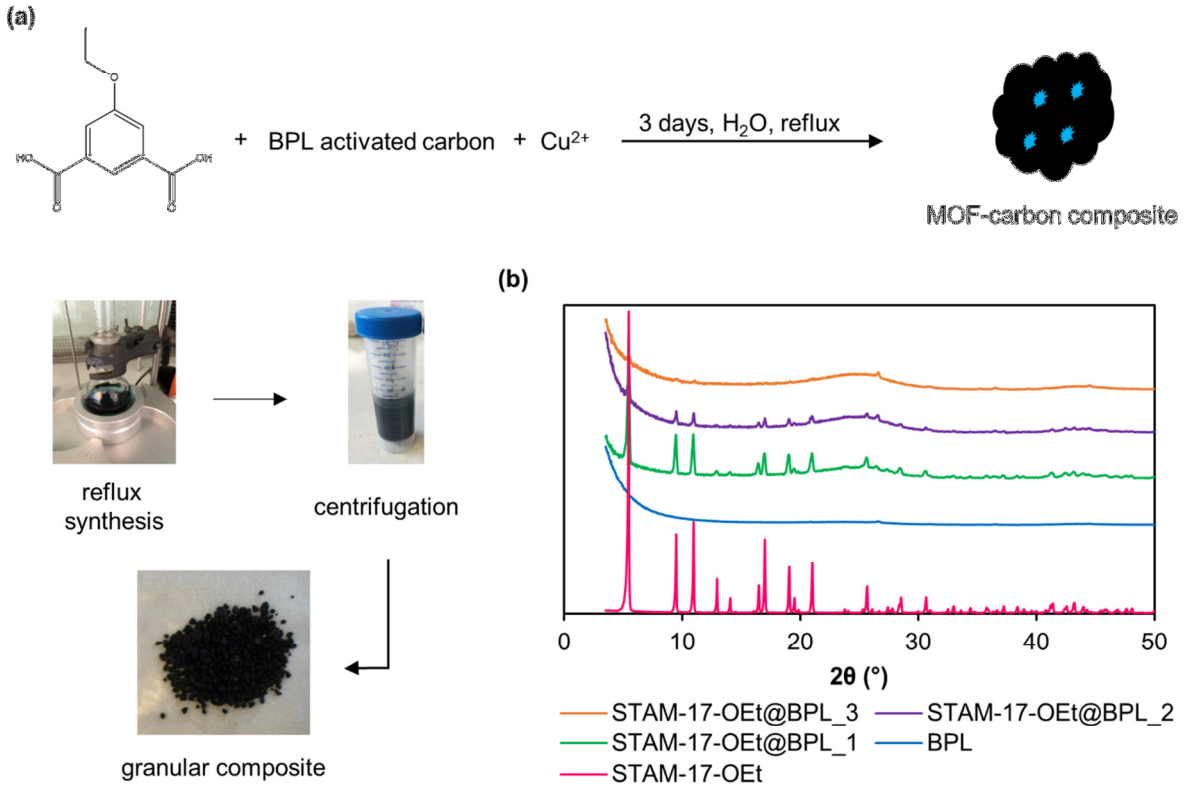

Figure 1. a) Synthesis of STAM-17-OEt@BPL composite materials; b) Powder X-ray diffraction patterns of the original MOF, unimpregnated BPL activated carbon and the three composites with varying weight percentages of MOF incorporation.

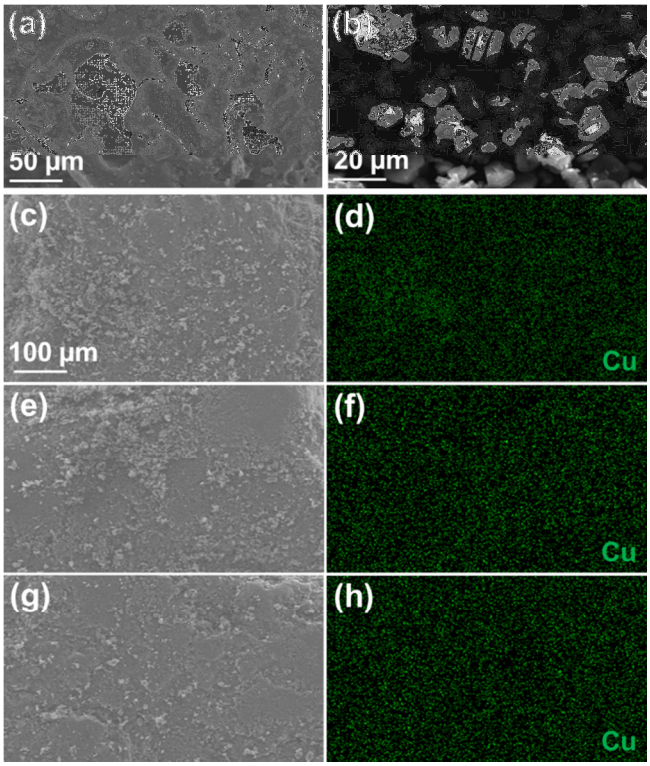

Figure 2. SEM images of: a,b) BPL activated carbon and STAM-17-OEt respectively; SEM image and copper elemental mapping image of: c,d) STAM-17-OEt@BPL_1; e-f) STAM-17-OEt@BPL_2; g,h) STAM-17-OEt@BPL_3.

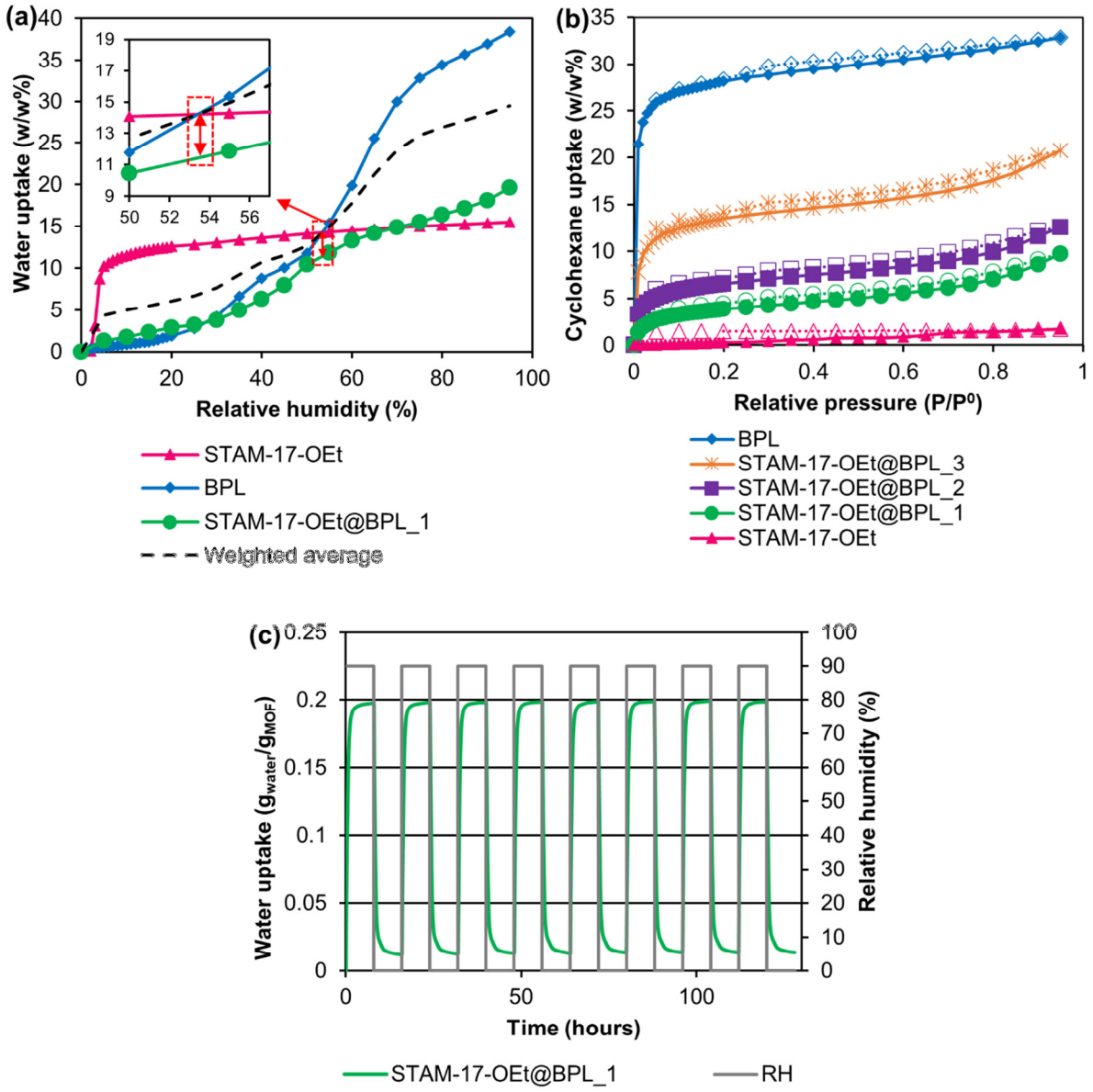

Figure 3. a) Adsorption branches of water isotherms displaying the shape difference and decrease in water uptake in the isotherm of STAM-17-OEt@BPL_1; b) Cyclohexane isotherms of composites; c) Water sorption-desorption cycling plot of STAM-17-OEt@BPL_1.

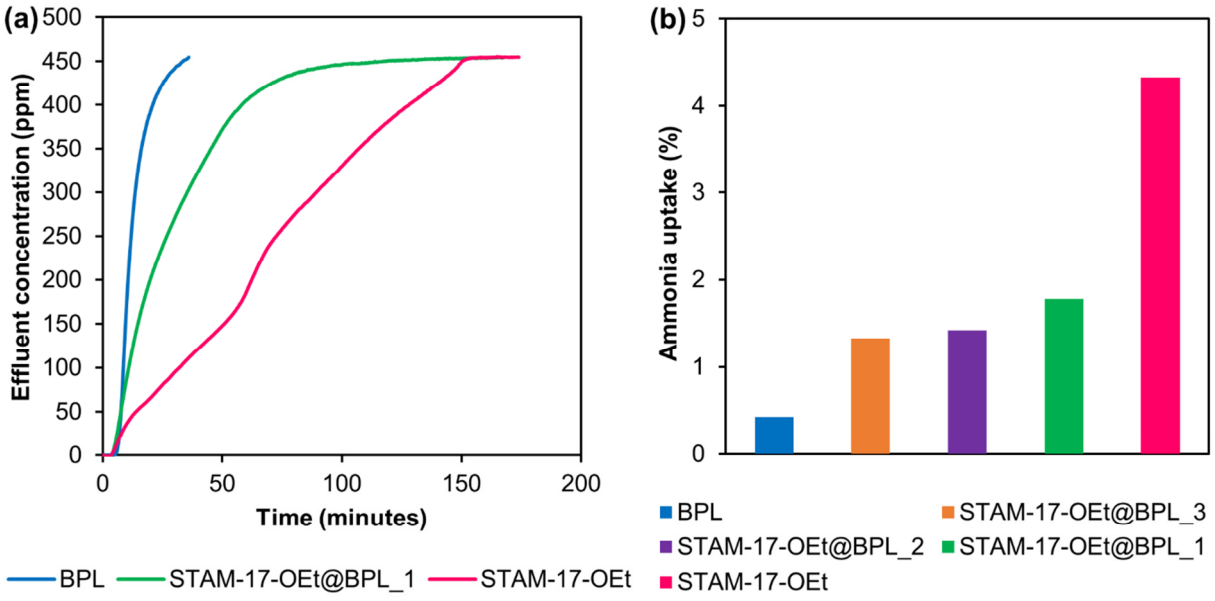

Figure 4. a) Ammonia micro breakthrough curves of BPL activated carbon, STAM-17-OEt and STAM-17-OEt@BPL_1; b) Ammonia uptake across the STAM-17-OEt@BPL series.

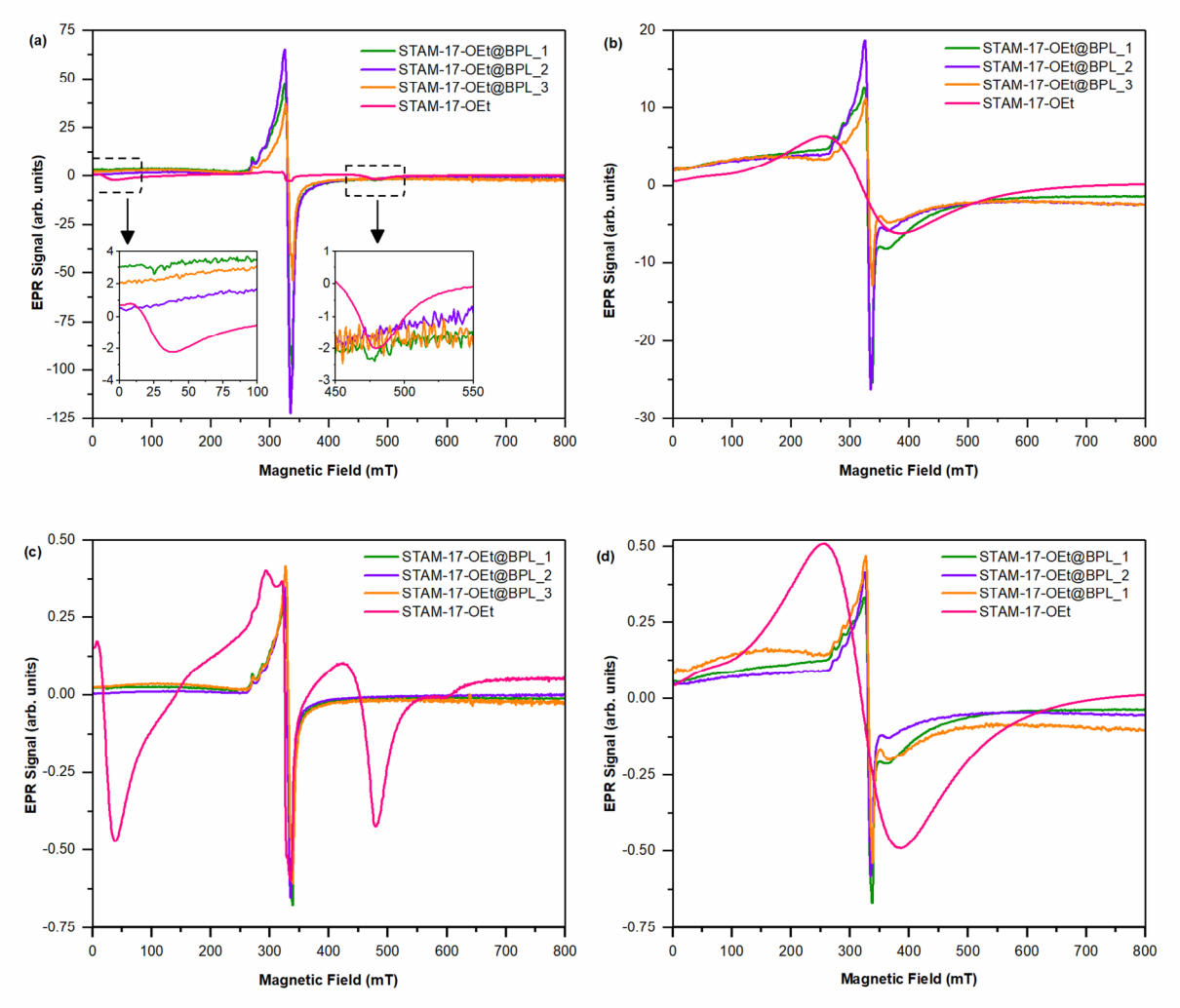

Figure 5. a,b) EPR spectra normalized by the estimated mass of STAM-17-OEt in each sample at 77 K and 300 K respectively; c,d) EPR spectra normalized by the peak-to-peak amplitude of the central resonance line at 77K and 300 K respectively.

Table 1. BET surface areas of STAM-17-OEt, BPL activated carbon and the three STAM-17-OEt@BPL composites.

Material	BET Surface Area [m^2/g]
STAM-17-OEt	58(1)
STAM-17-OEt@BPL_1	116(1)
STAM-17-OEt@BPL_2	188(2)
STAM-17-OEt@BPL_3	323(2)
BPL activated carbon	1209(7)

A new series of MOF-activated carbon composite materials are synthesised, using the copper MOF: STAM-17-OEt and commercially available BPL activated carbon. STAM-17-OEt is grown inside BPL carbon at three loadings to provide a series of granular materials that display excellent gas adsorption properties and water stability - offering an alternative to the currently used activated carbons in air purification systems.

Porous materials

L. N. McHugh*, A. Terracina, P. S. Wheatley, G. Buscarino, M. W. Smith, R. E. Morris*

Metal-organic Framework-Activated Carbon Composite Materials for Air Purification

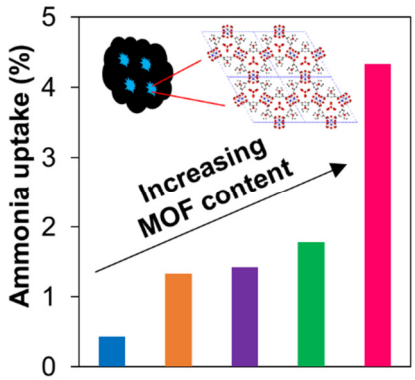

Supporting Information

Metal-organic Framework-Activated Carbon Composite Materials for Air Purification

Lauren McHugh*, Angela Terracina, Paul Wheatley, Gianpiero Buscarino, Martin Smith and Russell Morris*

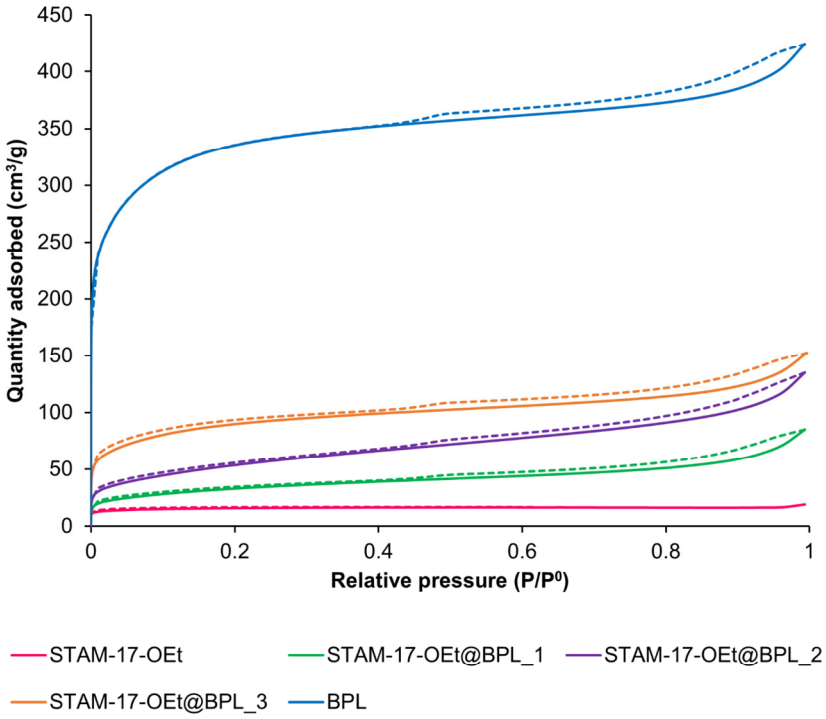

Figure S1. Nitrogen isotherms recorded at 77 K of STAM-17-OEt, STAM-17-OEt@BPL_1, STAM-17-OEt@BPL_2, STAM-17-OEt@BPL_3 and BPL activated carbon. Solid lines represent adsorption and dashed lines represent desorption.

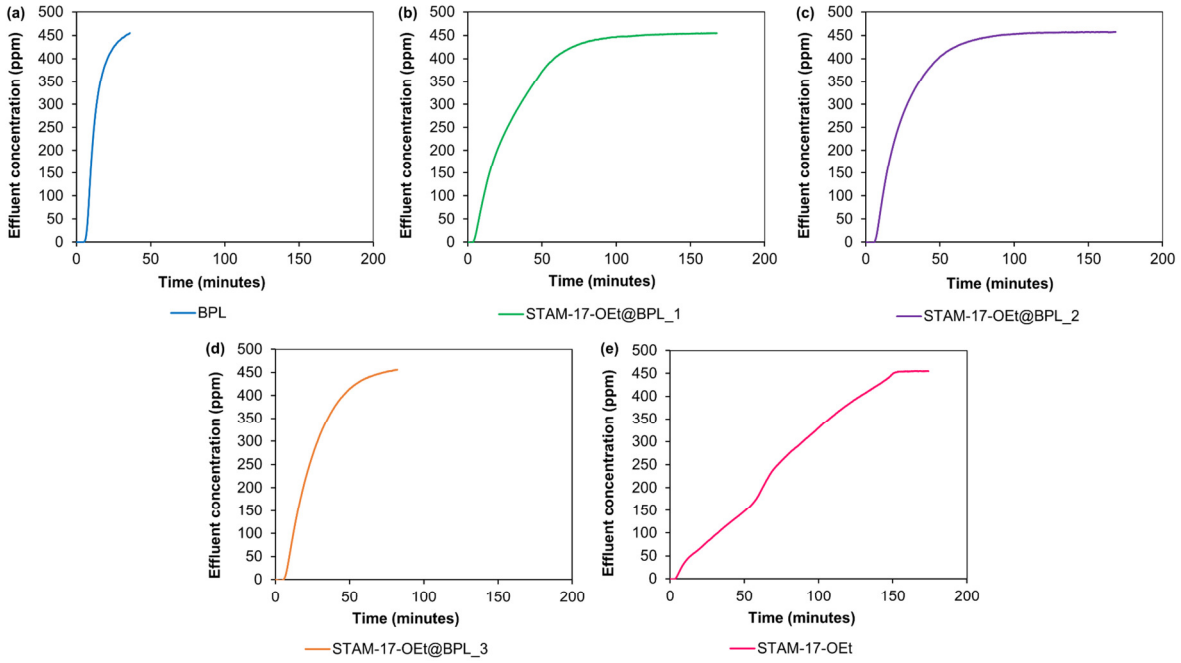

Figure S2. Ammonia micro breakthrough curves of a) BPL activated carbon; b) STAM-17-OEt@BPL_1; c) STAM-17-OEt@BPL_2; d) STAM-17-OEt@BPL_3; e) STAM-17-OEt.

Table S1. Percentage of ammonia removed from airstream based on weight of sample for BPL activated carbon, the three STAM-17-OEt@BPL composites and STAM-17-OEt.

Material	Ammonia uptake [%]
STAM-17-OEt	4.33
STAM-17-OEt@BPL_1	1.78
STAM-17-OEt@BPL_2	1.42
STAM-17-OEt@BPL_3	1.33
BPL activated carbon	0.43